Modeling and experiment of gas desorption of bubble column with an external loop in the heterogeneous flow regime

Hanjin Im, Jeil Park, and Jae W. Lee[†]

Department of Chemical and Biomolecular Engineering, KAIST, 291 Daehak-ro, Yuseong-gu, Daejeon 34141, Korea

Abstract−This work introduces an external loop to a bubble column and presents enhanced gas exchange in the heterogeneous flow regime. Gas exchange experiments under the same amount of gas input were carried out with varying gas velocity to understand the difference of bubble characteristic between the bubble column (BCR) and the bubble column with an external loop (BCR-EL). The observation of rise and descending velocity of bubbles in the BCR-EL showed that the fraction of bubbles passing the downcomer continuously increases with the incremental superficial gas velocity. A gas molecule in the liquid phase is desorbed by another gas molecule, and this gas exchange was assumed to be a phenomenon that a reactant in the liquid phase is converted to a product. To test the validity of the assumed gas exchange as a reaction in the experiments with the BCR-EL, a modeling study was performed using Fisher-Tropsch synthesis. It prevailed that the syngas conversion was higher in the BCR at the homogeneous flow regime, while the BCR-EL at the heterogeneous flow regime (above 0.08 m/s) had higher syngas conversion than the BCR due to higher gas recycle to the downcomer.

Keywords: Bubble Column, Bubble Column with an External Loop, Homogeneous Flow Regime, Heterogeneous Flow Regime

INTRODUCTION

A bubble column reactor (BCR) [1-4], which is a multiphase reactor such as the fixed bed [5-9], moving bed [10], gas-liquid-liquid reactor [11], and fluidized bed reactor [12-14], has attracted interest in many industrial fields due to its simple operation, good gas-liquid mass transfer, and low operating cost. It has a cylindrical main body and a gas sparger at the bottom of the column. Through the sparger, gas is distributed and gas-liquid flow is developed. In the bubble column operation, there are two types of flow regimes: homogeneous and heterogeneous [15,16]. The homogeneous regime is observed at a low superficial gas velocity. At this regime, a uniform size distribution of bubble is obtained. Each bubble has a uniform rise velocity, and limited frequencies of bubble coalescence occur [17]. At a typical superficial gas velocity higher than 0.05 m/s, the flow property changes to the heterogeneous regime (or churn-turbulent) [18]. A large input of gas phase results in the creation of large bubbles in this regime. Turbulent motion and vigorous mixing of the gas bubbles induce frequent bubble breakup and coalescence [19]. Thus, a broad distribution of bubble size can be obtained.

An airlift reactor is a specific type of the BCR [20], and named after that a liquid circulation is lifted by air input. It is divided into two separate zones: the riser and the downcomer. The riser is where the gas sparger is normally installed. Thus, gas is distributed at the riser, and the downcomer is where the moving direction of liquid is downward by the liquid circulation. Each separated zone has a

different condition in the gas holdup, liquid-phase mass transfer coefficient, and circulation velocity. The airlift reactor has an internal loop or external loop [21]. For the internal loop airlift reactor, an internal wall separates the riser and the downcomer. The external loop airlift reactor has an additional circulation path horizontally attached to the main body column at the top and the bottom. This external loop airlift reactor has the same design with the bubble column reactor with an external loop (BCR-EL).

Although the BCR-EL has a structure similar to the BCR, different hydrodynamics and flow patterns can be observed due to the external loop [22,23]. In BCR, the riser and the downcomer exist in a single cylindrical column; however, both of them are separated in the BCR-EL. Because the position of riser and downcomer has an important role in the internal liquid circulation, the circulation velocity is crucial in understanding the hydrodynamics of the BCR-EL. The two types of column were compared in terms of both internal liquid circulation velocity and mass transfer parameters [22,24, 25]. The performance of the BCR-EL was analyzed with respect to the cross-sectional area ratio of downcomer to riser (A_d/A_r). In case of the mass transfer parameter, it was reported that the gas holdup and the volumetric mass transfer coefficient of the BCR-EL ($A_d/A_r>0$) were smaller than the bare BCR ($A_d/A_r=0$). When it comes to the liquid circulation velocity, the increase in A_d/A_r can increase the liquid circulation velocity [22,23]. Details of the reaction profile can be obtained using these empirical hydrodynamic parameters in the reactor modeling.

Modeling analyses of the BCR were carried out in many previous literatures [26-28] using Fischer-Tropsch synthesis and glycerol hydrochlorination, while direct chlorination of ethylene was investigated in the BCR-EL [29]. The reactor modelling connected the

flow behaviors with the mass and energy balances of the multiphase system. They used an axial dispersion model to interpret the BCR. The axial dispersion model employed a given empirical parameter (axial dispersion coefficient) to predict gas-liquid hydraulics and there are many case studies for the BCR [26-29]. However, the modelling study of the BCR-EL and the understanding of its performance relative to the bare BCR case have been very limited.

Thus, the main purpose of this work was to elucidate the comparative performance between BCR and BCR-EL through a modeling study by considering the same liquid phase volume in the two systems. The gas holdup was experimentally determined for each system and the final dissolved oxygen concentration was measured with the variation of the superficial gas velocity for the fixed total gas input. It was demonstrated that through steady-state dissolved oxygen (DO) measurements, the reaction conversion could increase with the rising superficial gas velocity, even in the heterogeneous regime if we assume that the oxygen depletion is equivalent to its consumption in the reaction. The bubble rise velocity was also measured to determine how many bubbles can pass over the external loop. After the experimental analysis, modeling of both BCR and BCR-EL was carried out to compare the performance between the two systems.

METHOD

1. Bubble Column Set Up

A detailed scheme of the bubble column experiment is illustrated in Fig. 1. The riser part of the bubble column is an acrylic column that has 0.2 m diameter and 1.8 m height. For the downcomer part, the body of the column has 0.1 m diameter and 1.2 m height. For the connection part between the riser and the downcomer, the length is 0.2 m and the diameter is 0.1 m. At the bottom of the riser column, a ring sparger with 54 holes with 0.001 m in diameter was installed to provide a consistent distribution of the gas phase. The gas sparger is made of 3/8" stainless steel pipe and has a
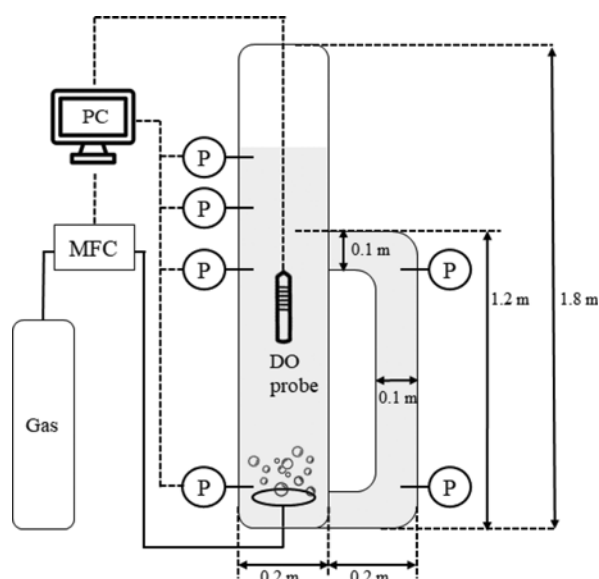
0.12 m diameter. A mass flow controller (MFC-Korea, TSCD245, Korea) was used to provide the gas phase. The superficial gas velocity was set to more than 0.01 m/s to avoid gas weeping near the sparger. To cover both homogeneous and heterogeneous flow regime, the superficial gas velocity was varied up to 0.133 m/s. To detect a pressure during the experiment, six pressure sensors (Sensys, PHPG 0003BCTG, Korea) that offer ±0.035% precision under the range of 0-3 bars were installed at different axial positions. Dynamic MFC and pressure signals were continuously recorded and the data were delivered to the PC.

2. Measurement Method

For the liquid phase, tap water and pure oxygen/nitrogen were used as gas and liquid phases. All experiments were at atmospheric pressure and room temperature. The liquid phase was filled before the experiment and the gas phase was injected through the sparger by the MFC. In this work, the batch operation of the bubble column was carried out. The pressure difference (Δp) between the two levels of the column, measured by pressure probes mounted with the wall, yields the mean gas holdup between these levels:

$$\Delta p = (1 - \varepsilon_G)\rho_l g \Delta z \qquad (1)$$

The pressure indicators were installed at the bottom and the top of both riser and downcomer for the accurate measurement of the gas holdup. A polarographic dissolved oxygen (DO) probe (Hanna Instruments, HI98193, USA) was used for measuring gas desorption. Oxygen gas was initially saturated in the liquid phase and then nitrogen was supplied to measure the remaining DO concentration.

The bubble velocity was measured by a stopwatch. For the rise bubble velocity, the exact time recording began once the bubble was released above the gas sparger. Then, the elapsed time was taken until the bubble passed a specific destination (axial position H/D=5). Because it is difficult to differentiate which bubble is being measured exactly, the first released bubble upon operation was observed. For the downcomer bubble velocity, the elapsed time was recorded until the bubble passed from the top to the bottom of the downcomer.

RESULTS AND DISCUSSION

1. Gas Holdup Observation

While some previous literatures compare between the BCR and the BCR-EL with the same liquid height but different liquid phase volumes, we compared the gas holdup between them using the same volume of the liquid phase [24,30,31], because the reactor size or liquid holdup matters for the exact comparison of gas holdup regardless of the reactor geometry. The aspect ratio (H/D) of experiment employing the BCR-EL was 5.3. For the bare BCR experiment, the aspect ratio was equal to 7.0, which makes the same liquid volume between the two. The observation of the gas holdup is displayed in Fig. 2. The riser gas holdup in the BCR-EL was smaller than the gas holdup of the bubble column. The result was in line with the result of the previous study where the column height had almost no effect on the gas holdup if the aspect ratio was larger than 5 [32].

2. Gas Desorption Experiments

To provide more detailed comprehension, the degree of gas desorption was determined. The pre-dissolved oxygen gas in the col-
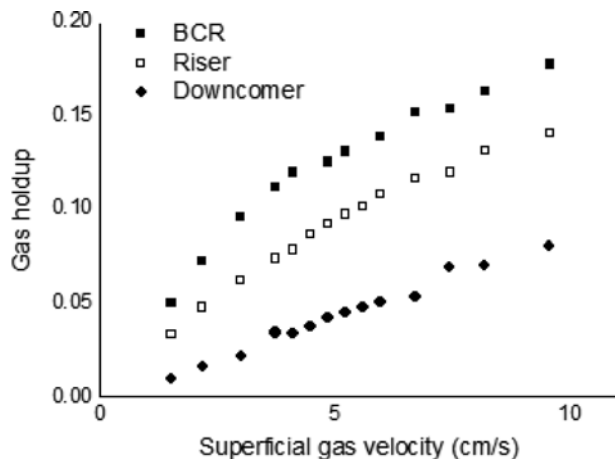

Fig. 1. Schematic diagram of the BCR-EL.

Fig. 2. Investigation of the gas holdup in the BCR and the BCR-EL (riser and downcomer).

umn will be desorbed if another gas is distributed to the gas sparger. This desorption event that the dissolved gas is replaced by the input gas was assumed as a reaction that a reactant in the liquid is replaced by a reaction product. In this manner, the amount of depletion of dissolved gas, or the difference of the initial and final dissolved gas concentration, can be interpreted as how far the reaction has progressed. This experiment was to understand how the gas concentration would change when the total volume of the gas was fixed and the superficial gas velocity was varied.

The oxygen gas was provided enough to the column before the experiment and the saturated concentration of the oxygen was 40 mg/L. Then, the nitrogen gas was distributed to the sparger and the variation of DO was measured. The added volume of the nitrogen was 47 L at the standard condition. In this experiment, the lower final DO means higher reaction conversion. The experimental result is shown in Fig. 3. The BCR with an aspect ratio of 5.3 was also investigated because the gas-liquid mixture overflowed at the high superficial gas velocity with an aspect ratio of 7.0. Both in the bare BCR and the BCR-EL, the final DO concentration decreased up to the superficial gas velocity of 0.041-0.048 m/s and then started
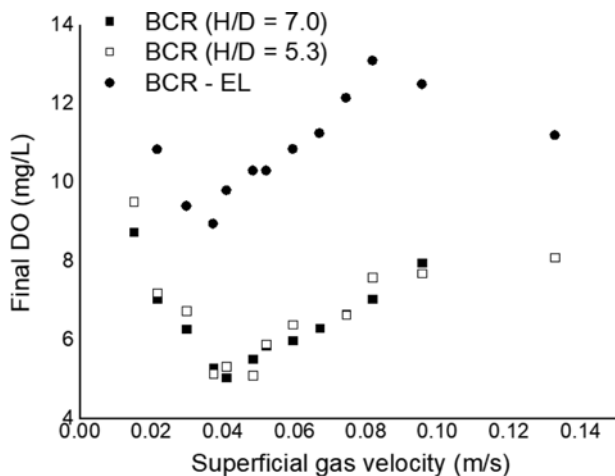
to increase with the increasing superficial gas velocity. If we assume the oxygen desorption from the liquid phase as the reactant depletion from the liquid phase in a reaction, the increasing reaction conversion trend can be expected until the superficial gas velocity reaches this value, and the decreasing reaction conversion trend would be observed after 0.048 m/s. The transition point can be inferred as the position of the transition regime since the bubble hydrodynamic is suddenly changed.

However, in the experiment using the BCR-EL, the trend was different. From 0.048 to 0.082 m/s, the final DO concentration tended to increase. Above a superficial gas velocity of 0.082 m/s, the final DO concentration decreased while the continuous rising trend of the final DO concentration was obtained in the bare BCR. This means that the reaction conversion can grow even in the high superficial gas velocity using the BCR-EL. Experiments covering superficial gas velocity above 0.133 m/s could not be carried out because the gas-liquid mixture overflowed.

3. Determination of Bubble Rise and Descending Velocity

Both bubble rise and descending velocity were measured to determine whether the final DO concentration had lower values in the BCR-EL than the BCR at the heterogeneous regime. As shown in Fig. 4, the bubble velocity was smaller in the downcomer than the riser in all the range of superficial gas velocity. All the bubble velocity was continuously growing with the increasing superficial
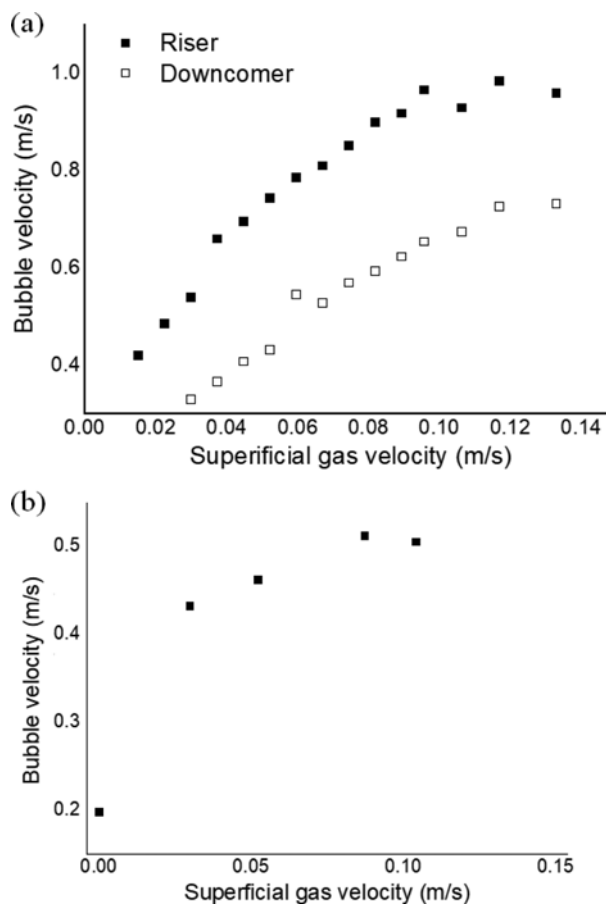

Fig. 3. Oxygen gas desorption investigation with fixed nitrogen input.

Fig. 4. (a) Bubble rise (riser) and descending (downcomer) velocity in the BCR-EL (b) Bubble rise velocity in the BCR.
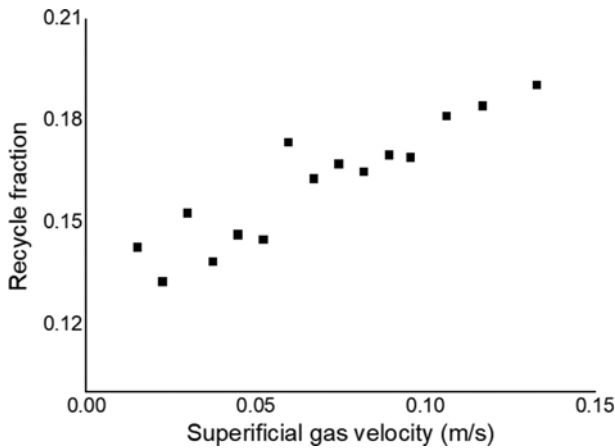
Fig. 5. Recycle fraction (degree of how many bubbles pass through downcomer) in the BCR-EL.

gas velocity. If a bubble in the riser travels up the column, there are two destinations: the downcomer and the top exit of the BCR-EL. Thus, a portion of bubbles entering the downcomer can be obtained using bubble velocity of both riser and downcomer, and we called this portion as a recycle fraction.

To find how many bubbles pass through the downcomer zone, the bubble recycle fraction was calculated by the ratio of the downcomer bubble velocity to the riser bubble velocity. The determined value is illustrated in Fig. 5. The fraction of the bubble traveling the downcomer continuously increased as the superficial gas velocity increased. If a bubble enters the downcomer, the residence time of the bubble is more than two-times than that of a bubble that does not pass the downcomer. A larger recycle fraction of the bubble can then be understood as better gas desorption. Thus, the final DO concentration was observed to decrease in the high superficial gas velocity zone as shown in Fig. 3.

By assuming gas desorption results as a gas reaction, this experiment revealed that higher input gas velocity could give higher reaction conversion in the BCR-EL even in the heterogeneous regime. However, since it is uncertain whether the trend of reaction conversion obtained by the reactor modeling matched with the results of the gas desorption experiments, the reaction conversion of the BCR and BCR-EL was compared through the reactor modeling in the following section.

4. Modeling of BCR and BCR-EL

4-1. Reaction Kinetics

Fischer-Tropsch synthesis was chosen as the target reaction of the reactor modeling.

$$n\,CO + (2n+1)\,H_2 \rightarrow C_nH_{2n+2} + n\,H_2O \tag{2}$$
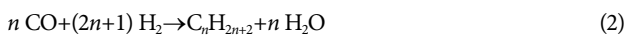
The Fischer-Tropsch synthesis is an important reaction in gas to liquid technology and coal liquefaction [33]. This process commonly uses supported iron or cobalt catalyst. In this work, the intrinsic kinetic equation by Yates and Satterfield was employed [34]. The equation was given as the Langmuir-Hinshelwood form,

$$-R_{CO+H_2} = \frac{a \cdot p_{H_2} \cdot p_{CO}}{(1+b \cdot p_{CO})^2} \tag{3}$$

where

$$a = 2.59218 \times 10^{-9} \exp\left(-\frac{37366.442}{8.314T}\right)\frac{mol}{s\,kg_{cat}bar^2} \tag{4}$$

$$b = 1.24298 \times 10^{-12} \exp\left(\frac{68474.9354}{8.314T}\right)1/bar. \tag{5}$$

4-2. Hydrodynamics of the BCR and BCR-EL

The homogeneous and heterogeneous regime can be found in operating both BCR and BCR-EL. Thus, the gas holdup and the volumetric mass transfer coefficient should be obtained in both regimes. For the gas holdup prediction in the BCR, following equations are as shown below [35]:

In the homogeneous flow regime:

$$\varepsilon_G = 0.883\rho_G^{0.143}\rho_L^{-0.0071}\mu^{-0.0012}\sigma^{-0.276}u_G^{0.8422} \tag{6}$$

In the heterogeneous flow regime:

$$\varepsilon_G = 1.04584\rho_G^{0.187}\rho_L^{-0.187}\mu^{-0.0631}\sigma^{-0.188}u_G^{0.557} \tag{7}$$

Experimental ranges of Eqs. (6) and (7) were ρ_G=0.16442−1.661 kg/m³, ρ_L=655−1027.71 kg/m³, μ=0.000326−0.001289 Pa·s, and σ= 0.0184−0.071 N/m.

The gas holdup correlation for the BCR-EL is shown below [22,36]:

$$\varepsilon_{G,r} = 0.465u_{G,r}^{0.65}\left[1+\left(\frac{A_d}{A_r}\right)\right]^{-1.06}\mu^{-0.103} \tag{8}$$

$$\varepsilon_{G,d} = 0.79\varepsilon_{G,r} - 0.057 \tag{9}$$

Eq. (8) was tested in a range of $\varepsilon_{G,r}$<0.17 and the tested range of Eq. (9) was $\varepsilon_{G,d}$<0.22.

The correlation to predict the volumetric mass transfer coefficient was as follows [22]:

$$k_La = 0.005u_G^{0.52}D_{GL}^{0.5}\rho_L^{1.03}\left[1+\left(\frac{A_d}{A_r}\right)\right]^{-0.85}\mu^{-0.89}\sigma^{-0.75} \tag{10}$$

This correlation was tested for the following conditions: 0.03<u_G< 0.26 m/s and 0<A_d/A_r<0.444.

Thus, this equation can be used in both homogeneous and heterogeneous regime. In Eq. (10), D_{GL} is the diffusion coefficient of the liquid phase. The diffusion coefficient was calculated from the following correlation [37]:

$$D_{GL} = 8.93 \times 10^{-6}\frac{v_G^{1/6}}{v_L^{1/3}}\left[\frac{P_L}{P_G}\right]^{0.6}\frac{T}{\mu} \tag{11}$$

The axial dispersion coefficient was calculated using the following correlations [38]:

$$D_{eff,L} = 0.31\,V_LD_c \tag{12}$$

For the BCR case,

$$V_L = 0.21(gD_c)^{\frac{1}{2}}\left(\frac{u_G^3\rho}{g\mu}\right)^{\frac{1}{8}} \tag{13}$$

For the BCR-EL case [39],

$$V_{L,r} = \frac{0.23u_{G,r}^{0.32}\left(\frac{A_d}{A_r}\right)^{0.97}\mu^{-0.39}}{(1-\varepsilon_r)} \tag{14}$$

$$V_{L,d} = \frac{0.23u_{G,d}^{0.32}\left(\frac{A_d}{A_r}\right)^{-0.03}\mu^{-0.39}}{(1-\varepsilon_d)} \quad (15)$$

$$V_{L,r} = \frac{u_{G,r}}{(1-\varepsilon_{G,r})}, \quad V_{L,d} = \frac{u_{G,d}}{(1-\varepsilon_{G,d})} \quad (16)$$

4-3. Model Equation of the BCR and BCR-EL

Governing equations of the axial dispersion model for the BCR are as follows [27].

Momentum balance:

$$\frac{dp}{dz} = -g(\varepsilon_G\rho_G + \varepsilon_L\rho_L) \quad (17)$$

Overall mass balance (gas phase):

$$\frac{du_G}{dz} = u_G\left(\frac{1}{T}\frac{dT}{dz} - \frac{1}{p}\frac{dp}{dz}\right) - \frac{R_GT_R}{p}\Sigma_{i=1}^{N}(k_La)_i(c_{i,L}^* - c_{i,L}) \quad (18)$$

Mass balance (component i, gas phase):

$$\varepsilon_GD_{eff,G}\frac{d^2c_{i,G}}{dz^2} = u_G\frac{dc_{i,G}}{dz} + c_{i,G}\frac{du_G}{dz} - (k_La)_i(c_{i,L}^* - c_{i,L}) \quad (19)$$

Mass balance (component i, liquid phase):

$$\varepsilon_LD_{eff,L}\frac{d^2c_{i,L}}{dz^2} = -(k_La)_i(c_{i,L}^* - c_{i,L}) - \varepsilon_L\nu_iR \quad (20)$$

This one-dimensional axial dispersion model considers the two first-order nonlinear differential equations (momentum balance and overall mass balance) and the two second-order nonlinear differential equations for each component (mass balance of component i in both gas and liquid phase). Although the bare governing equation has another energy balance, isotherm reaction was assumed in this work to simplify the model as in the previous studies [40, 41].

For the BCR-EL modeling, the governing equation is the same as in the BCR for the riser. An additional term in mass balance of liquid phase was added since gas-liquid flow is countercurrent in the downcomer:

$$\varepsilon_{L,d}D_{eff,L,d}\frac{d^2c_{i,L,d}}{dz^2} = -u_{L,d}\frac{dc_{i,L,d}}{dz} \quad (21)$$
$$-(k_La)_{i,d}(c_{i,L,d}^* - c_{i,L,d}) - \varepsilon_{L,d}\nu_iR$$

As for the boundary condition, BCR and BCR-EL have different boundary conditions. Details of the boundary condition are summarized in Table 1. The numbers '0' and '1' are the reactor bottom and the reactor top, respectively.

Table 1. Boundary conditions for governing equation (0: lower boundary, 1: upper boundary)

BCR case

$$\left(\frac{u_Gp}{R_GT}\right)(0) = \frac{\dot{N}_G(0)}{A}$$

$$\left(u_Gc_{i,G} - \varepsilon_GD_{eff,G}\frac{dc_{i,G}}{dz}\right)(0) = \frac{\dot{N}_{i,G}(0)}{A}$$

$$\left(\frac{dc_{i,L}}{dz}\right)(0) = 0$$

$$\left(\frac{dc_{i,G}}{dz}\right)(1) = 0, \quad \left(\frac{dc_{i,L}}{dz}\right)(1) = 0,$$

$$p(1) = p_{rxn}$$

BCR-EL case

Riser

$$\left(\frac{u_{G,r}p_r}{RT}\right)(0) = \frac{\dot{N}_G(0)}{A_r} + \frac{u_{G,d}p_d}{R_GT}(0)$$

$$\left(u_{G,r}c_{i,G,r} - \varepsilon_{G,d}D_{eff,G,d}\frac{dc_{i,G,r}}{dz}\right)(0) = \frac{\dot{N}_{i,G}(0)}{A_r}$$

$$\left(u_{L,r}c_{i,L,r} - \varepsilon_{L,r}D_{eff,L,r}\frac{dc_{i,L,r}}{dz}\right)(0) = (u_{L,d}c_{i,L,d})(0)$$

$$\left(\frac{dc_{i,G,r}}{dz}\right)(1) = 0$$

$$\left(u_{L,r}c_{i,L,r} + \varepsilon_{L,r}D_{eff,L,r}\frac{dc_{i,L,r}}{dz}\right)(1) = (u_{L,d}c_{i,L,d})(1)$$

$$p_r(1) = p_{rxn}$$

Downcomer

$$u_{G,d}p_d(0) = u_{G,r}p_r(0)$$

$$\left(\frac{dc_{i,G}}{dz}\right)(0) = 0$$

$$\left(u_{L,d}c_{i,L,d} + \varepsilon_{L,d}D_{eff,L,d}\frac{dc_{i,L,d}}{dz}\right)(0) = (u_{L,r}c_{i,L,r})(0)$$

$$\left(\frac{dc_{i,G,d}}{dz}\right)(1) = 0$$

$$\left(u_{L,d}c_{i,L,d} + \varepsilon_{L,d}D_{eff,L,d}\frac{dc_{i,L,d}}{dz}\right)(1) = (u_{L,r}c_{i,L,r})(1)$$

$$p_d(1) = p_{rxn}$$

4-4. Modeling Results

The modeling equations were solved using MATLAB software. The modeling result was validated before comparing the performance of the BCR and the BCR-EL. There were several literatures

Table 2. Validation of the modeling result with experimental data of previous literature [39]

Case no.	Experimental condition			CO conversion (%)		
	Temperature (°C)	Pressure (bar)	Space velocity (L/gcat·h)	Experimental	Modeling	Deviation (%)
Case 1	230	10	1.8	78.04	70.8	9.28
Case 2	245	10	2.4	93.03	85.3	8.31
Case 3	255	10	3.0	90.78	91.1	0.35
Case 4	270	10	3.6	93.95	95.1	1.24

covering the experimental result of the Fischer-Tropsch synthesis with a slurry phase reactor [40,42,43]. However, there have very few available experimental results with the BCR. Thus, the experimental result from the fixed-bed reactor was employed in the validation of the modeling result [43]. Fisher-Tropsch synthesis is usually investigated in the pressurized condition (1.0-3.0 MPa). Since a proper hydrodynamic correlation of the BCR-EL for the pressurized condition has not been investigated in the literature, the experimental result at 1.0 MPa [43] was used. The comparison between modeling and experimental result is summarized in Table 2 [43]. Because the fixed-bed reactor and the BCR have different geometries, there are some differences in CO conversion between modeling and experimental results. However, the difference is within an acceptable range of 10%.

To compare the performance between the BCR and the BCR-EL, the operating condition and the properties of the catalyst are shown in Table 3. The dimension of the BCR and the BCR-EL was the same as the experimental apparatus used in this modeling investigation. Simulations were carried out in following conditions: u_G=0.0149–0.133 m/s and ε_s=0.1. Modeling of Fisher-Tropsch synthesis in the BCR was usually at 0.2-0.4 of ε_s [28,38]. This solid phase hold-up can affect hydrodynamics in the BCR and the BCR-

EL. However, relatively few studies have been devoted to the gas holdup correlation of the riser and the downcomer in the presence of the solid phase in the BCR-EL. Thus, a small amount of solid phase was assumed to minimize the error of the gas holdup. In Fig. 6, syngas conversions in both BCR and BCR-EL are illustrated. In the low superficial gas velocity, the syngas conversion of the BCR is higher than that of the BCR-EL. At the superficial gas velocity higher than 0.074 m/s, the BCR-EL has higher syngas conversion than the BCR and the conversion gap between the BCR and the BCR-EL is continuously increasing to the superficial gas velocity of 0.133 m/s. An identical trend was found in the previous literature when the BCR was compared with the airlift reactor [31]. Although the flow regime transition from homogeneous to heterogeneous region occurred earlier in the airlift reactor, the gas residence time of the airlift reactor was greater than that of the BCR. It was also greater in the airlift reactor than the BCR, although slug flow was dominant in the airlift reactor and the BCR showed a heterogeneous flow. The separation of the riser and the downcomer enables longer gas residence time even in the disadvantageous mass transfer region of homogeneous and slug flows. Therefore, in the homogeneous flow regime below 0.074 m/s, the BCR has better performance than the BCR-EL, but the trend is opposite in the heterogeneous regime.

Figs. 7 and 8 illustrate a detailed view of syngas conversion with respect to the dimensionless axial position. In the homogeneous regime, the syngas conversion at the reactor bottom is higher in the BCR than the BCR-EL in the axial position of the riser. However, in the heterogeneous regime, the syngas conversion at the reactor bottom is higher in the BCR-EL than BCR. Although the syngas conversion is similar at the reactor top, the gap of the syngas conversion becomes large as moving down to the reactor bottom. This conversion gap can be explained by the high gas input to the downcomer. In the high superficial gas velocity region, a large amount of the gas passes through the downcomer. The converged product at the downcomer travels to the entrance of riser in the same way as at the reactor bottom. At the superficial gas velocity of 0.106 m/s, the syngas conversion difference between the two types at the reactor bottom is larger than that at the superfi-

Table 3. Operating conditions of modeling and catalyst properties

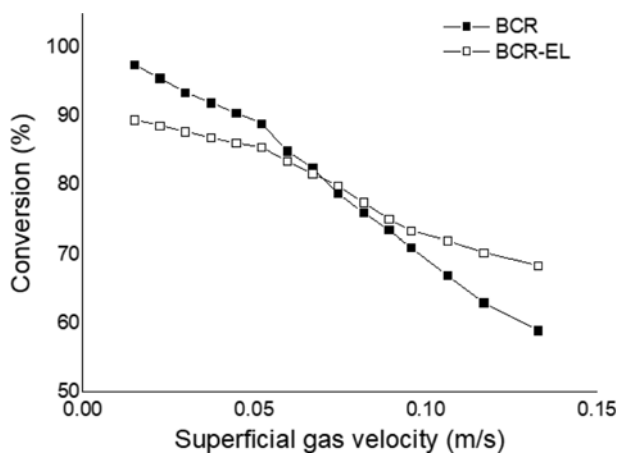|	
Operating conditions	
Column pressure	0.1 MPa
Column temperature	220 °C
Column (riser) height	1.8 m
Downcomer height	1.2 m
Column diameter	0.2 m
Downcomer diameter	0.1 m
Catalyst holdup	0.1
H_2/CO ratio	2
Catalyst properties (Co/SiO₂)	
Bulk density	0.38 g/mL
Surface area	257 m²/g
Pore volume	1.2 mL/g

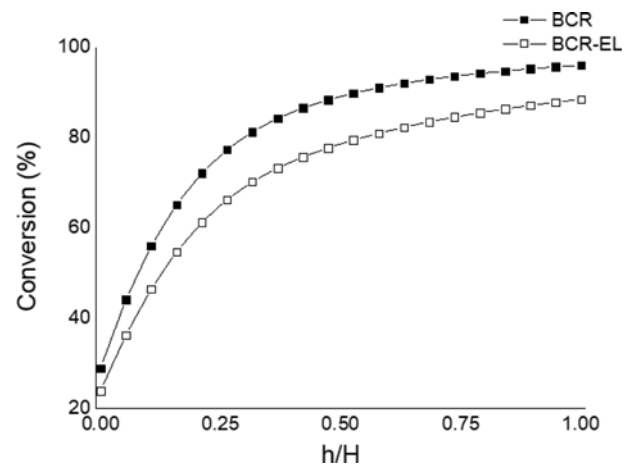Fig. 6. Syngas conversion of the BCR and the BCR-EL (modeling results).

Fig. 7. Axial profile of the syngas conversion at superficial gas velocity of 0.0223 m/s (modeling results).
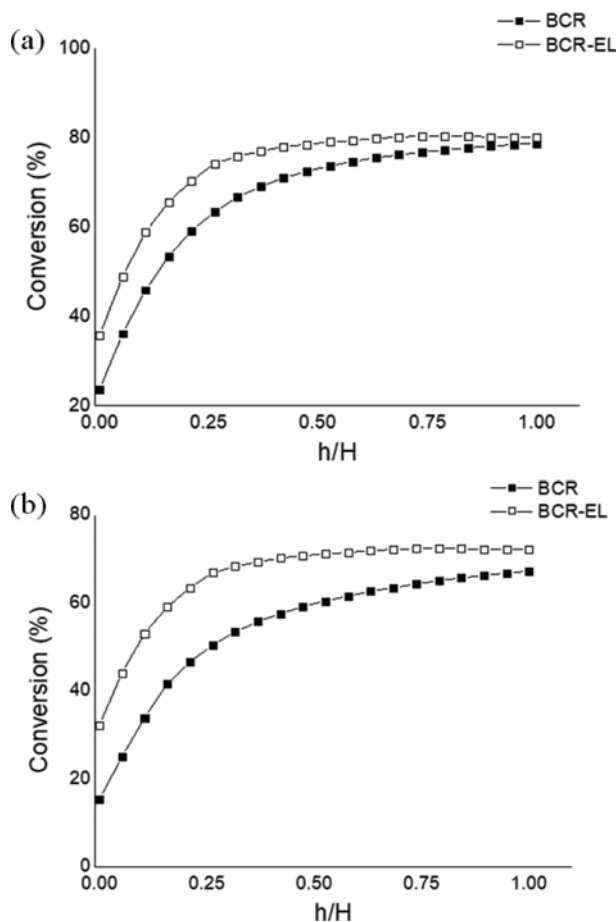
Fig. 8. Axial profile of the syngas conversion in the heterogeneous regime (modeling results) (a) Superficial gas velocity of 0.074 m/s (b) Superficial gas velocity of 0.106 m/s.

cial gas velocity of 0.074 m/s (see Fig. 8). Thus, the BCR-EL has a potential option for high reaction conversion at the high superficial velocity of the heterogeneous regime.

CONCLUSION

This work has demonstrated that through gas desorption experiments, the BCR-EL has a potential to provide a higher reaction conversion than the BCR. The reason for the higher conversion is that the fraction of bubbles heading for the downcomer from the riser continuously increase with the incremental superficial gas velocity. For a sophisticated comparison, a reactor modeling with the Fisher-Tropsch synthesis reaction showed that in the homogeneous regime, the BCR had better performance than the BCR-EL, while the BCR-EL had higher syngas conversion in the heterogeneous regime due to more gas recycle to the downcomer.

ACKNOWLEDGEMENT

NOMENCLATURE

A : cross-sectional area of column [m^3]
c : concentration [mol/m^3]
D : diffusion coefficient [m^2/s]
D$_c$: column diameter [m]
D$_{eff}$: axial dispersion coefficient [m^2/s]
g : gravitational acceleration [m/s^2]
H : liquid height [m]
kg$_{cat}$: catalyst mass [kg]
k$_L$a : volumetric mass transfer coefficient [1/s]
$\dot{N}$: molar flow rate [mol/s]
P : parachor [g$^{1/4}$cm^3/g mol s$^{1/2}$]
p : pressure [bar]
R : reaction rate [mol/m^{3}s]
R$_G$: gas constant [J/mol K]
T : temperature [K]
u : superficial velocity [m/s]
V : liquid linear velocity [m/s]
v : molal volume at its normal boiling point [cm^3/g mol]
z : axial position [m]

Greeks Letter
ε : phase holdup
μ : liquid viscosity [Pa·s]
ν : stoichiometric coefficient
ρ : density [kg/m^3]
σ : surface tension [N/m]

Subscript
d : downcomer
eff : effective
G : gas
L : liquid
r : riser
rxn : reaction
S : solid

REFERENCES

1. W.-D. Deckwer, Y. Louisi, A. Zaidi and M. Ralek, *Ind. Eng. Chem. Process Des. Dev.*, **19**, 699 (1980).
2. J. H. Yang, Y. G. Hur, H.-T. Lee, J.-I. Yang, H.-J. Kim, D. H. Chun, J. C. Park, H. Jung and S. B. Park, *Chem. Eng. Res. Des.*, **90**, 1457 (2012).
3. L. Vafajoo, H. Savoji, R. Fayal and A. Baghaei, *Korean J. Chem. Eng.*, **28**, 1727 (2011).
4. S. Cvetkovic, B. Bugarski and B. Obradovic, *Korean J. Chem. Eng.*, **35**, 324 (2018).
5. H. S. Lim, D. Kang and J. W. Lee, *Appl. Catal. B*, **202**, 175 (2017).
6. J. Park, S. Lee and J. W. Lee, *Ind. Eng. Chem. Res.*, **57**, 2310 (2018).
7. J. Park, R. H. Kang and J. W. Lee, *Korean J. Chem. Eng.*, **34**, 1763 (2017).
8. R. H. Kang, J. Park, D. Kang and J. W. Lee, *Korean J. Chem. Eng.*, **35**, 734 (2018).
9. B. Todic, M. Mandic, N. Nikacevic and D. B. Bukur, *Korean J.*

Chem. Eng., **35**, 875 (2018).

10. M. Yi and J. W. Lee, *Korean J. Chem. Eng.*, **33**, 3401 (2016).

11. J. W. Lee, S. Hauan, K. M. Lien and A. W. Westerberg, *Proc.: Mathematical, Phys. Eng. Sci.*, **456**, 1953 (2000).

12. J. W. Lee, Y. Ko, Y. Jung, K. Lee and E. Yoon, *Comput. Chem. Eng.*, **21**, S1105 (1997).

13. L. Wei, Y. Lu, J. Zhu, G. Jiang, J. Hu and H. Teng, *Korean J. Chem. Eng.*, **35**, 2117 (2018).

14. J.-R. Lee, N. Hasolli, S.-M. Jeon, K.-S. Lee, K.-D. Kim, Y.-H. Kim, K.-Y. Lee and Y.-O. Park, *Korean J. Chem. Eng.*, **35**, 2321 (2018).

15. A. Shnip, R. Kolhatkar, D. Swamy and J. Joshi, *Int. J. Multiphase Flow*, **18**, 705 (1992).

16. H. Im, S. Lee and J. W. Lee, *Chem. Eng. Res. Des.*, **136**, 654 (2018).

17. G. R. Guédon, G. Besagni and F. Inzoli, *Chem. Eng. Sci.*, **161**, 138 (2017).

18. A. Schumpe and G. Grund, *Can. J. Chem. Eng.*, **64**, 891 (1986).

19. C. O. Vandu, K. Koop and R. Krishna, *Chem. Eng. Sci.*, **59**, 5417 (2004).

20. J. B. Joshi, V. V. Ranade, S. D. Gharat and S. S. Lele, *Can. J. Chem. Eng.*, **68**, 705 (1990).

21. C. Vial, E. Camarasa, S. Poncin, G. Wild, N. Midoux and J. Bouillard, *Chem. Eng. Sci.*, **55**, 2957 (2000).

22. M. K. Popovic and C. W. Robinson, *AIChE J.*, **35**, 393 (1989).

23. K. H. Choi and W. K. Lee, *J. Chem. Technol. Biotechnol.*, **56**, 51 (1993).

24. N. Bendjaballah, H. Dhaouadi, S. Poncin, N. Midoux, J.-M. Hornut and G. Wild, *Chem. Eng. Sci.*, **54**, 5211 (1999).

25. Y. Chisti and M. Moo-Young, *Biotechnol. Bioeng.*, **34**, 1391 (1989).

26. C. A. de Araujo Filho, D. Mondal, S. Haase, J. Wärnå, K. Eränen, J.-P. Mikkola and T. Salmi, *Chem. Eng. Sci.*, **149**, 277 (2016).

27. S. Schluter, A. Steiff and P.-M. Weinspach, *Chem. Eng. Process.*, **31**, 97 (1992).

28. C. Maretto and R. Krishna, *Catal. Today*, **52**, 279 (1999).

29. J. A. Orejas, *Chem. Eng. Sci.*, **54**, 5299 (1999).

30. T.-G. Byun, A.-P. Zeng and W.-D. Deckwer, *Bioprocess. Eng.*, **11**, 167 (1994).

31. B. Jin and P. Lant, *Chem. Eng. Sci.*, **59**, 2379 (2004).

32. X. Luo, D. Lee, R. Lau, G. Yang and L. S. Fan, *AIChE J.*, **45**, 665 (1999).

33. G. P. Van Der Laan and A. Beenackers, *Catal. Rev.*, **41**, 255 (1999).

34. I. C. Yates and C. N. Satterfield, *Energy Fuels*, **5**, 168 (1991).

35. H. Im, J. Park and J. W. Lee, *ACS Omega*, **4**, 1329 (2019).

36. R. A. Bello, C. W. Robinson and M. Moo-Young, *Biotechnol. Bioeng.*, **27**, 369 (1985).

37. M. T. Tyn and W. F. Calus, *J. Chem. Eng. Data*, **20**, 106 (1975).

38. R. Krishna, J. Van Baten, M. Urseanu and J. Ellenberger, *Chem. Eng. Sci.*, **56**, 537 (2001).

39. M. Popović and C. W. Robinson, *Biotechnol. Bioeng.*, **32**, 301 (1988).

40. A. Outi, I. Rautavuoma and H. S. van der Baan, *Appl. Catal.*, **1**, 247 (1981).

41. B. Sarup and B. Wojciechowski, *Can. J. Chem. Eng.*, **67**, 62 (1989).

42. A. Sari, Y. Zamani and S. A. Taheri, *Fuel Process. Technol.*, **90**, 1305 (2009).

43. N. Moazami, M. L. Wyszynski, H. Mahmoudi, A. Tsolakis, Z. Zou, P. Panahifar and K. Rahbar, *Fuel*, **154**, 140 (2015).